Quantifying Geothermal Resource Potential and Uncertainty Analysis using a Natural State Model of Kotamobagu Geothermal Field in North Sulawesi, Indonesia

Bei B.R. Nagoro[1], John O'Sullivan[1]

[1]Department of Engineering Science, The University of Auckland, Private Bag 90120, Auckland, New Zealand

bnag352@aucklanduni.ac.nz

Keywords: *Geothermal resource potential, uncertainty quantification, 3D natural state model, geothermal reservoir modelling*

ABSTRACT

Kotamobagu Geothermal field, located in North Sulawesi, Indonesia is expected to hold significant potential as a geothermal energy resource. This study presents a calculation of its resource potential using an uncertainty analysis and a natural state model. Through the utilization of publicly available reports and data, a comprehensive 3D geological model of the field has been constructed. This process was followed by setting up a numerical model that was used to simulate the steady state of the geothermal system. Many sample models were run and conditioned against the limited data and this process was used to determine the reservoir potential.

The construction of the 3D geological model involved the integration of geology, geophysics, geochemical and spatial data using LEAPFROG Geothermal. Based on this, a numerical model was developed that is compatible with both AUTOUGH2 and Waiwera. The model was calibrated by adjusting the permeability and upflow to simulate the natural state of the geothermal reservoir. Next, 1000 samples of possible alternative models were generated based on the distribution of upflow and the rock permeabilities and simulated using high-performance computing facility. These samples were then filtered using the estimated temperature below the clay cap. Finally, the filtered samples were used to estimate the resource potential by applying a production algorithm.

The results show a range of reservoir temperature from 200-250°C with applying 109 kg/s upflow. The model estimates that the upflow of heat arises underneath Mt. Ambang and along the northeast-southwest trending faults. Additionally, the same family of faults at the east side of the volcano acts as a barrier preventing the fluid from seeping out. The filtering process resulted in 213 sample models which were used in the Approximate Bayesian Computation (ABC) to show that the P90, P50, and P10 estimates of power outputs are 70 MWe, 160 MWe, and 270 MWe, respectively, for the 25 years of simulated production.

1. INTRODUCTION

The National Energy General Plan (RUEN) of Indonesia targets the production of 10 GWe from geothermal by 2030 and further increases to 17.5 GWe in 2050, thus a robust exploration of potential fields and optimization of the development plan in existing projects should be conducted. A total estimated geothermal potential of up to 27.7 GWe spread across the country is thought to support the plan.

Kotamobagu geothermal field is situated in North Sulawesi Province, Indonesia. It lies across 124°07'14" E - 124°29'19" E and 0°32'19" N - 0°53'1" N, approximately 200km southwest of Manado City, the capital of the province. Exploration surveys were undertaken in the 1980s and 2018, confirmed that the system has acidic features, such as fumaroles around the Mt. Muayat area (4km to the East of Mt. Ambang), and is surrounded by a large, neutral-pH Cl fluid with a liquid-dominated reservoir (Hochstein & Sudarman, 2008), resulting in an estimated of 80Mwe resource potential (Direktorat Panas Bumi, 2017).

This paper presents a significantly enhanced resource assessment through the utilization of uncertainty quantification and the natural state model, employing a 3-dimensional digital conceptual model of the Kotamobagu geothermal field. This approach aims to provide stakeholders with better economic insights to aid their decision-making process. The digital conceptual model is built from a geological and alteration model constructed using LEAPFROG Geothermal and the calibrated steady-state numerical model is generated by using AUTOUGH2. An ensemble of possible models based on the rock permeabilities and upflow distribution is then set up by

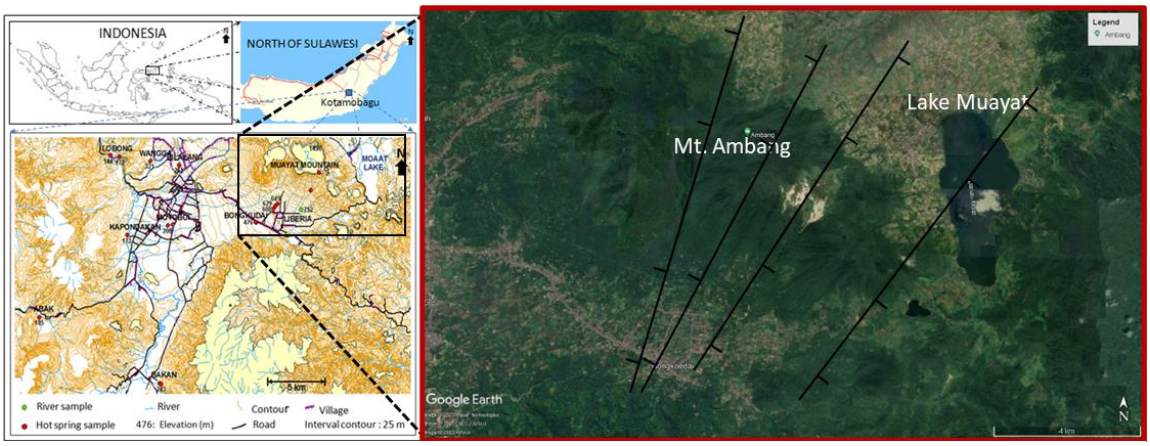

Figure 1: Location of Kotamobagu Area (modified from Riogilang et al., 2011 and (GoogleEarth, 2023))

Proceedings 45th New Zealand Geothermal Workshop
15-17 November, 2023
Auckland, New Zealand
ISSN 2703-4275

sampling parameter values, and the ensemble is used to construct a probability distribution of the resource potential.

2. FIELD INFORMATION

2.1 Geological Setting

Kotamobagu field is situated in the Minahasa Region, North Sulawesi. It comprises shallow to deep water marine sedimentary rocks, including carbonates and is overlain by andesitic volcanic rocks. The early Miocene strato-volcano formed a volcanic field centred mainly in the Muayat Caldera (Kavalieris et al., 1992). A report states that the collapse of this andesitic volcanism formed a large 16 km diameter caldera around the ring fractures (West Japan Engineering Consultants, 2007). Recent studies show that the Kotamobagu geothermal field is composed of Tertiary sediment rock and Quaternary sediment and volcanic rocks (Riogilang et al., 2012).

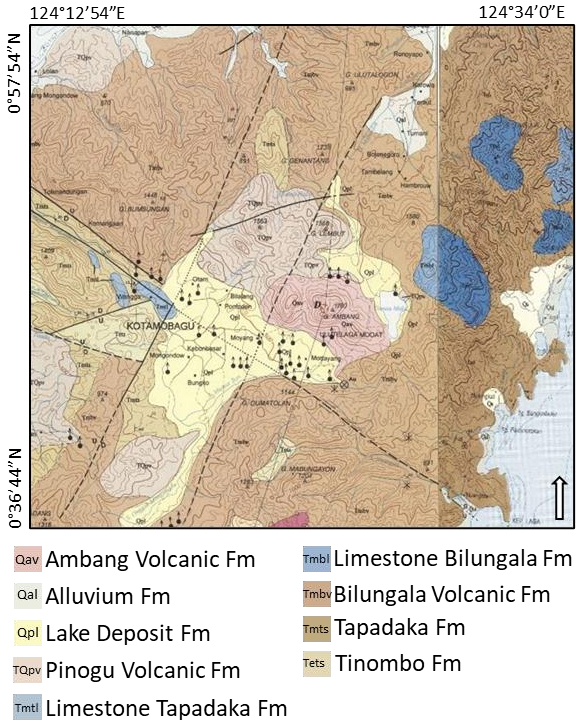

Figure 2: Geological map of Kotamobagu area (Modified from Apandi & Bachri, 1997).

Based on the geological map (Apandi & Bachri, 1997), the area of interest consists of various formations from the Eocene to Holocene/Recent era. The oldest formation is the Tinombo Formation in the Eocene era, overlayed by the Tapadaka Formation and Bilungala Formation in the Early to Late Miocene, continued by the Pinogu Formation in the Pliocene-Pleistocene era and superimposed by the recent Ambang Volcanic Formation in the Holocene era.

The geological structure in the Kotamobagu field is set as the consequence of active tectonism and vulcanism that formed the K-shape on Sulawesi Island due to the severe collision of the Australian and New Guinea plates (Katili, 1978). The subduction zone in the NW Sulawesi in the Quaternary period ignited the movement which formed the arc in the Northern Arm of Sulawesi in which Kotamobagu is located. As a result, it holds a complex structure feature with various fault directions dominated by Northeast-Southwest and Northwest-Southeast major faults with subordinate small discontinuous East-West faults.

2.2 Geophysics

A series of resistivity measurements have been conducted to identify the preliminary target and provide resistivity mapping under Mt. Ambang (A. Andan, 1982; Direktorat Panas Bumi, 2017). The first survey was done in 1980 using a number of Schlumberger resistivity traverses and Vertical Electrical Soundings (VES). The survey aims to get a shallow layer profile by covering approximately 100 km^2 around Mt. Ambang. The survey suggested that the low resistivity (5ohm-m) is related to the main thermal features which were believed to underlie Mt. Ambang.

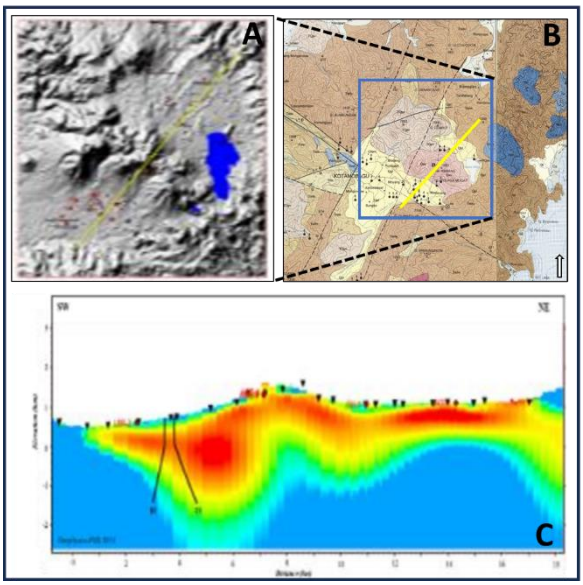

Figure 3: MT Survey line in topographic map (A), and geological map (B). Resistivity profile from Kotamobagu Geothermal Area (C).

A recent magnetotelluric survey in 2018 which was intended to give more detailed information and deeper profiling confirmed the existence of a low resistivity body underneath Mt. Ambang (Direktorat Panas Bumi, 2017). This is expected to be the cap layer zone. It forms a dome shape on its northern side and goes deeper to the south. The northeast side of the survey area also correlates to the early crater and is suggested to act as a permeability barrier for the system. This study is only using one available profile from the recent magnetotelluric survey.

2.3 Geochemistry

Water sample analyses from manifestation and river water around the Kotamobagu geothermal system have been examined (Riogilang et al., 2011b, 2011a, 2013). There are 25 samples in total taken to measure the water temperature, pH, electric conductivity, and anion-cation.

The water chemistry resulted from the analyses was divided into five main types of manifestation, namely acid sulphate type (MUAH-16), chloride-sulphate water type (LIBR-4; MUAH-15; MAKH-22,25), bicarbonate water type (LIBH-1,2,3; BONH-5; BILH-13; WANI-14; GUAH-21; KAKH-23), chloride water type (WULH-19,20), and hybrid water type (BAKH-6,7; ABAH-8; LOBH-9,10; KAPH-11; MOTH-12; INSH-7,18; WULR-24).

ISSN 2703-4275

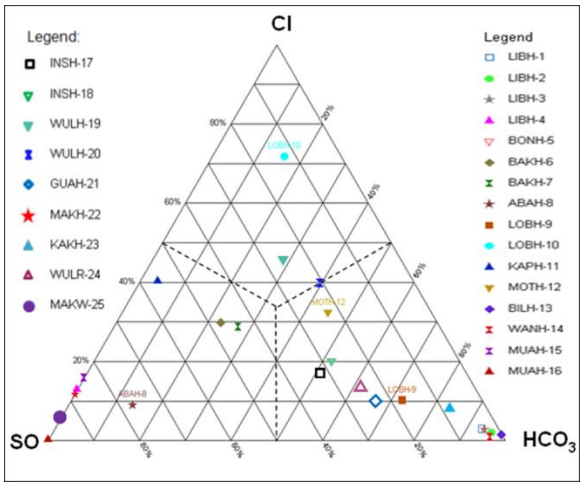

Figure 4: Ternary plot for Cl, SO4, and HCO3 (modified from Riogilang et al., 2011a, 2011b).

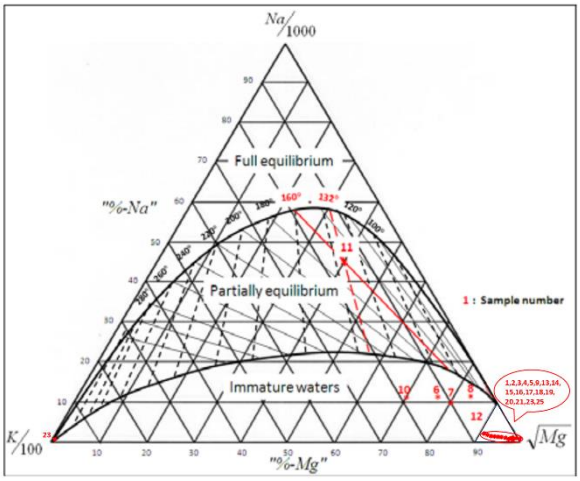

Figure 5: Ternary plot for Na-K-Mg (modified from Riogilang et al., 2011a, 2011b).

The surface temperature from manifestations varies from 24.7°C to 93.1°C, and the pH value ranges from 2.24 to 8.4 The type of feature changes from acidic, bicarbonate and chloride moving outward from the top of the volcano showing a typical high terrain volcanic geothermal system (Henley & Ellis, 1983).

The water geothermometer indicates a range of reservoir temperature from 88°C to 320°C. However, according to the ternary diagram, only one sample exhibits mature water and suggests partial equilibrium, indicating that the remaining samples are immature.

3. CONCEPTUAL MODEL

A hydrothermal conceptual model has been generated (Riogilang et al., 2013) and used for this paper as the initial concept in creating the updated 3D visualization. The deep geothermal fluid boils at depth and flows upward, resulting in H_2S gas and mixing with oxygen-rich surface water creating chloride sulphate water type through oxidation processes at the slope area and in the Makaroyen. They are represented by LIBR-4, MUAH-15, and MAKH-22,25 as low-pH - high-Cl surface manifestations. The dominant bicarbonate water feature around Mt. Ambang forms due to the high content of CO_2 gas from dissolved magmatic in the waters and interacts with the confining rocks and produces neutral pH bicarbonate water.

The acid sulphate at MUAH-16 is created by the high pressurized H_2S content from under the volcano. This is expected to be the source of heat for the system. The heat source has elevated the temperature of the overlaying permeable rock, which is now mixed with the deep hot fluid and meteoric water. This is reckoned as the consequence of the fault structure and fractures up to the surface acting as pathways for the fluid.

The initial temperature for the reservoir is thought to reach more than 200°C and is located in the Tertiary Volcanic rocks which are composed of andesitic lava and tuff. The depth of the reservoir zone is thought to be 800-2000 m below the surface. A low resistivity anomaly from the magnetotelluric survey suggests the possibility of an impermeable cap zone. It is expected as the result of a hydrothermal alteration process due to low-intermediate temperature with a dominant non-magmatic water source forming a propylitic alteration.

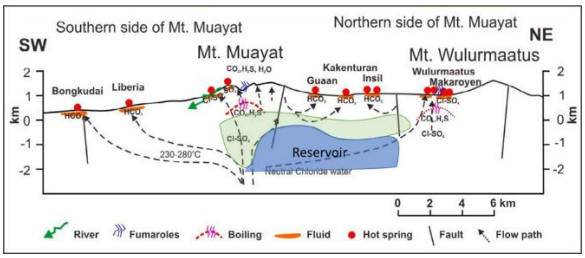

Figure 6: Conceptual model of the Kotamobagu geothermal area (modified from Riogilang et al., 2013).

4. METHODOLOGY

4.1 3D Model Construction

A geothermal conceptual model serves to depict and emphasizes key characteristics of the geology and the primary process involved in the system. It highlights the temperature distribution and fluid flow entering, circulating within, and exiting the system (Boseley et al., 2010; Cumming, 2009). To build an extensive conceptual model, a combination of geological, geophysical, and geochemical data is necessary.

4.1.1 Geological Model

The geological model began by extracting the X, Y, and Z coordinate to create the topography of the model. It is enclosed within 40 km of Mt. Ambang as the expected centre of the geothermal system. Extensive coverage aims to give enough volume so that the reservoir model can contain the large-scale convective system and its surrounding meteoric recharge. The rock stratigraphy and fault structure are set by digitizing the vertical and horizontal boundary for each formation and fault based on the geological map.

Rock Formation	Abbreviation	Geologic Age
Ambang Volcanic Fm	Qav	Holocene
Alluvium and Coastal Deposits	Qal	Holocene
Lake Deposits Fm	Qpl	Holocene

ISSN 2703-4275

Pinogu Volcanic	TQpv	Pliocene-Pleistocene
Limestone Tapadaka Fm	Tmtl	Late Miocene
Limestone Bilungala Fm	Tmbl	Late Miocene
Bilungala Volcanic Fm	Tmbv	Early Miocene
Tapadaka Fm	Tmts	Early Miocene
Tinombo Fm	Tets	Eocene

Table 1: Summary of the stratigraphy units in the Kotamobagu geothermal system.

Table 1 illustrates the geological period within the system, which is divided into five epochs: Eocene, Early Miocene, Late Miocene, Pliocene-Pleistocene, and Holocene eras (Apandi & Bachri, 1997). Among the formations mapped, the oldest is the Tinombo Fm, comprising shale and sandstone, with its primary outcrop located in the western part of Kotamobagu city (van Leeuwen & Muhardjo, 2005). The Tapadaka Fm consists of sandstone and greywacke, while the Bilungala Fm is comprised of volcanic breccia, andesite, and tuff (Apandi & Bachri, 1997). Bilungala Fm is known to extend across the northern arm of Sulawesi (Patuti et al., 2017). The volcanic breccia is believed to be the result of a significant ancient eruption, though the exact volcano responsible for its discharge remains unidentified (A. Andan, 1982).

The later deposition occurred during the Tertiary-Quaternary era, known as the Pinogu Volcanic, composed of lava and tuff (Kavalieris et al., 1992). In the more recent Holocene era, three formations accumulated: Lake Deposit, Coastal Deposit, and Ambang Volcanic (Apandi & Bachri, 1997). It is expected that the recent Ambang Volcanic holds a crucial role in the Kotamobagu geothermal system.

In the system, there are 10 active faults with assumed depths and dips that crosscut all formations vertically 90°. These assumptions are expected to give the optimum pathways for the fluid as there is no data to constraint. The main faults are in the NE-SW, NW-SE, and E-W directions. The NE-SW faults cross cuts Mt. Ambang and Mt. Mabungayon. It is thought to control the fluid flow from the heat source up to the surface manifestation near Liberia and Makaroyen villages. The E-W faults control the manifestation at the western part of the system at Bilalang and Lobong villages. A few faults are also added based on the alignment of the surface manifestation to capture its flow behaviour. This help to give a better understanding of the fluid flow and to optimise the calibration process in the numerical model.

4.1.2 Alteration Model

The clay cap zone was assigned on top of the reservoir as the top barrier for the fluid flow at a depth range from 250-2450m. It is estimated to be made of low permeability clays due to the rock alteration process. Resistivity profiles and maps were used as the basis for generating the alteration model. The same method of digitizing was used using polylines and points to create the boundary and determine the shape of the cap. Surface manifestations also play an essential role as a constraint for determining the lateral extent of the possible clay. The result is that it has an up-dome under the northern part of the clay cap, which makes the clay cap much thicker on this side and then it becomes thinner on the opposite side.

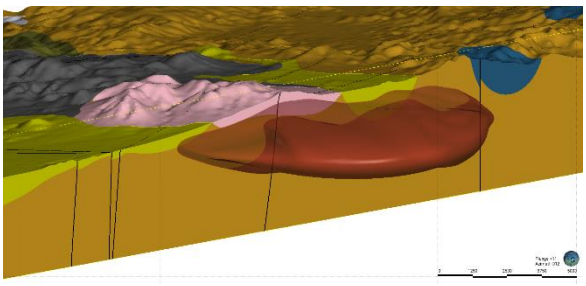

Figure 7: 3D combined model of geology, faults, and alteration zone on SW-NE slice. The red body represents a clay cap. Black line represent the faults and other volumes represent the rock formations.

4.2. Numerical Model

To simulate the natural state of the geothermal system, a numerical model must be set up and run using a geothermal simulator. A model grid is generated based on the 3D model and the boundary condition is also applied to govern the behaviour of the system.

4.2.1 Model Grid Setup

The grid was set to be 40° from the azimuth in order to be parallel with the main strike of the faults to ease the process of calibration. The grid model extends over an area of 23 km x 26 km with a total of 39,994 blocks. The size of the outer blocks is 1000 m x 1000 m with the vertical thickness varying between 500 m at the base and thinning to 100 m near the surface. A higher resolution was applied in the zone of interest with the size of blocks reduced to 500 m x 500 m.

The rock types of the blocks were automatically assigned to match the rock types from the Leapfrog model (Popineau et al., 2018).

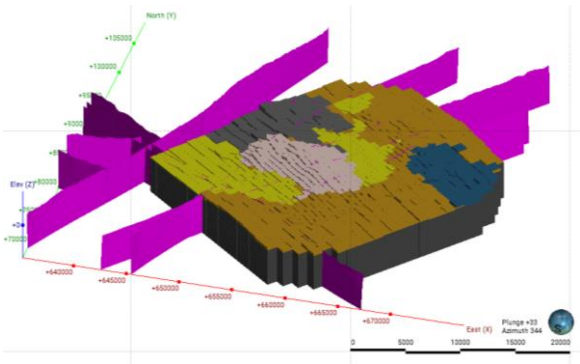

Figure 8: Grid layout for Kotamobagu geothermal area. Magenta lines are the fault in the system.

4.2.2 Boundary Condition

A dry atmospheric condition was assigned to the top surface of the model with a pressure and mean temperature of 1 bar and 21°C, respectively. The EOS3 module was used to give the thermophysical properties of water and air as input for mass and energy balance equations (Pruess et al., 1999). This allows the model to include the vadose zone above the water table which is at close to atmospheric pressure. High permeability was assigned to the top surface blocks to allow

ISSN 2703-4275

rainwater infiltration to flow to lower elevations following the topography. An annual rainfall of 2,340mm with a 10% infiltration rate was applied.

No-flow boundary condition at the side was adopted because the model is large enough to include the whole convective geothermal system with no side flows.

A uniform background heat flux of 80mW/m2 is applied to represent the upflow zone at the base of the model. Additionally, hot mass is injected into 17 blocks, generating a total upflow of 109 kg/s with an enthalpy of 1400 kJ/kg located under NE-SW faults which cross Mt. Ambang.

4.3. Natural State Simulation

4.3.1 Model Calibration

This paper used manual calibration based on adjusting the hot mass injected at the base of the model and the permeabilities of the rock types governing the fluid flow. The natural state model was run for $5x10^{14}$ seconds simulation time to achieve steady-state conditions. Hot mass was produced from 17 generator blocks located under NE-SW faults which cross Mt. Ambang. These faults are expected to play a major role in controlling the fluid flow and convection in the Kotamobagu geothermal system. The NE-SW faults also provide permeability along the strike of the faults to allow outflows to the southwest. They also act as barriers to flow across their strike confining flow to the northwest and southeast. Thus, the calibrated fault permeability should allow for increased permeability along the strike and up the dip of faults but only decreased permeability across the strike of a fault.

The clay cap properties were assigned at depth 250m down to 2450m with an estimated overall thickness of 2000 m following the shape of the resistivity anomaly from the magnetotelluric results and were set to have low permeability.

4.4 Resource Assessment

The results from the natural state model are used as a starting point for calculating the resource potential. The rock type and properties, fault information and upflow information are crucial for creating many models based on random sampling parameters, to perform test runs and choose a smaller number of steady-state geothermal models. Here we apply a new method that has been established to perform geothermal resource assessment by including advanced numerical geothermal modelling and uncertainty quantification to incorporate reservoir physics, wellbore physics, and realistic energy extraction scenarios (Dekkers et al., 2022a).

4.4.1 Parameter Sample

Parameters used in generating the samples were the magnitude and distribution of upflow and the rock permeabilities. The total upflow was sampled from a Gaussian distribution with the calibrated upflow as a mean. The total upflow was then distributed over the selected upflow blocks on the faults with a spatial correlation between the blocks.

The permeability samples used are based on the four main rock types in the model (De Beer et al., 2023). The calibration process results in the permeability of the rocks being defined by a combination of the formation permeabilities with modifiers to represent the alteration or structural setting. The modifiers were constrained to follow geological rules. To illustrate, the modifier is set at least 1 or higher for fault rock permeability along the strike and up the dip to prevent the permeability from decreasing in those directions. In contrast, inverse concept is applied to the permeability across the fault and to the alteration rock. The sampling process generates 1000 sample models which were simulated using a high-performance computing facility of the New Zealand eScience Infrastructure (NeSI).

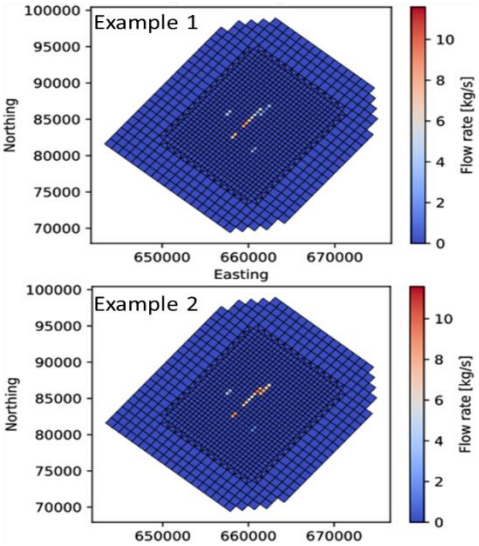

Figure 9: Sets of sampled upflows in the blocks on the bottom layer of the model.

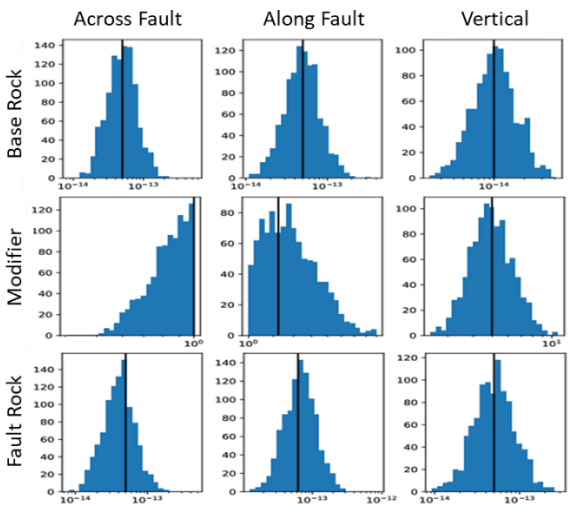

Figure 10: Permeability distribution of the Tertiary Dacite (top) multiplied by the modifier (middle) resulting in the fault rock (Fault B) (bottom).

4.4.2 Samples Conditioning

Once the models have been generated by sampling and all the models have been run to steady-state, the next step is to condition the sample models on the temperature at locations under the clay cap using the Approximate Bayesian Computation (ABC), which it aims to filter the sample based on the proximity of the selected blocks to reach a certain constraint (Dekkers et al., 2022b). A total of 125 blocks are used for conditioning and they are located under the dome shape of the clay cap on the northern side. These blocks are expected to best represent the temperature that controls the alteration zone and are assumed to reach around 190°C. The

ISSN 2703-4275

best samples show that the temperature reaches 190°C directly under the clay cap.

The distribution follows the shape of the alteration zone while following the imposed geological rules. The worst samples, on the other hand, show that some of the models result in low-temperature distribution, while the others exceed the appointed temperature up to the top of the alteration zone. In total, there are 213 accepted samples from 896 converged natural state model that will be used in the production scenario.

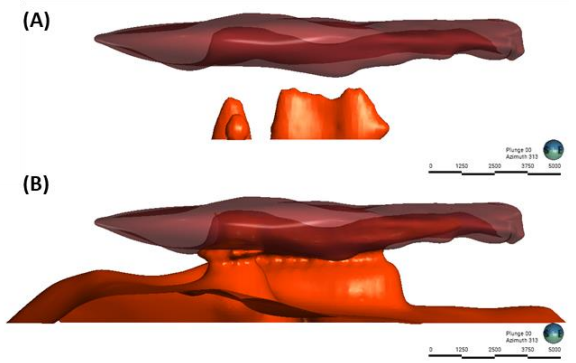

Figure 10: Comparison of the worst sample (A) and the best sample (B). The red body represents the clay cap and orange layer represent the temperature distribution at 190°C.

5. RESULT

5.1 Natural State Model

Surface manifestation temperature and estimated temperature below the clay cap are used to calibrate the steady-state model. The surface manifestations used are focused on the top side and slope of Mt. Ambang, namely LIBR-4; MUAH-15,16, and MAKH-22,25. The measured temperature is expected to be higher than the model temperature at the surface block due to the grid size which is approximately up to 500 m x 500 m, making each block far larger than any surface feature, and the value calculated is the average temperature of that block. However, the upflow and outflow sections from the model already depict similar conditions as the data.

The MUAH-16 indicates that the upflow from the heat source directly seeps out from the bottom and produces acid sulphate feature on top of Mt. Ambang with pH of 2.25. The outflow is indicated by the presence of bicarbonate water and chloride sulphate manifestations situated at the slope of Mt. Ambang and some were found further NE from the volcano. The bicarbonate water was found only at the northern side of the volcano and is thought to appear due to high CO_2 content absorbed in the steam and condensed into groundwater and has a neutral pH of 8. The chloride sulphates found in both the southern and northern sides of the volcano are expected to come from the H_2S gas from the boiling geothermal fluid that is mixed with oxygen-rich surface water. The calibrated model resulted in a reservoir temperature range from 200°C-250°C as a result of 109 kg/s upflow.

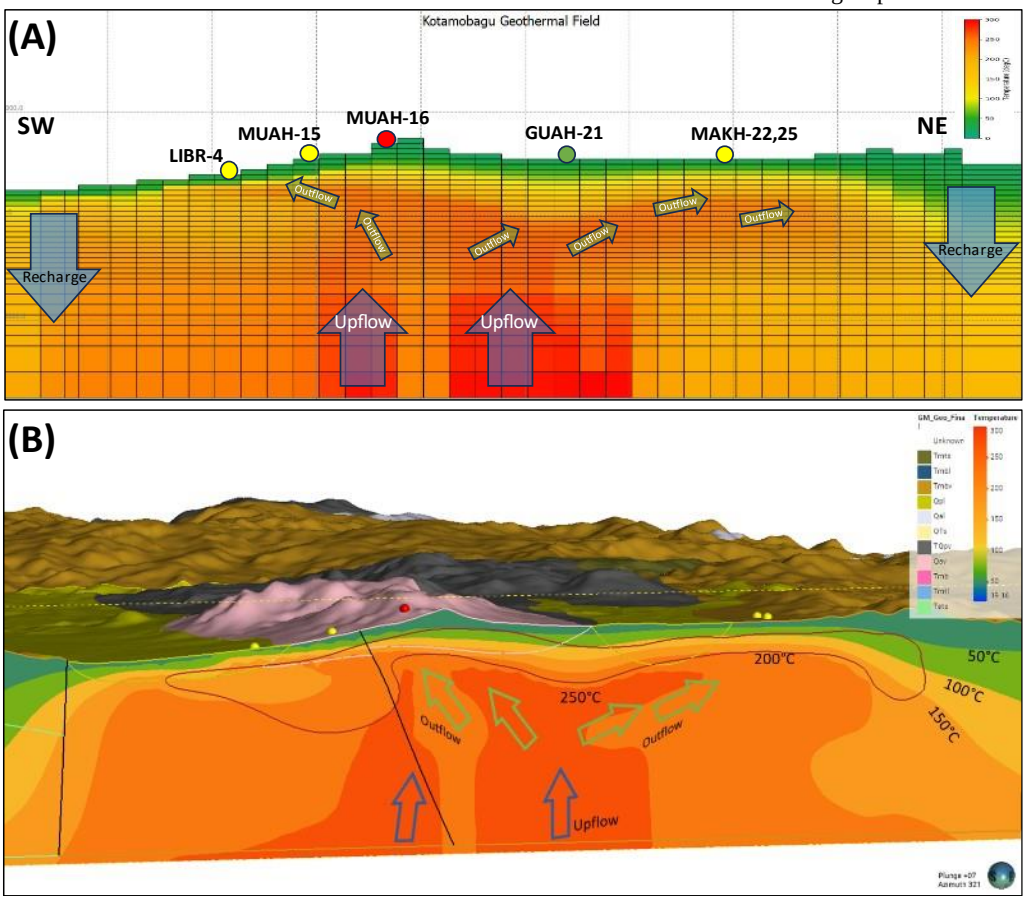

Figure 92: Temperature distributions, mass flow, rock information, surface manifestations, and alteration zone in grid layers (A) and 3D model (B)

ISSN 2703-4275

The heat and mass flowing to the northeast side is due to the shape of the clay cap and fault structure. The permeability controls the fluid flow which allows it to leak at the surface. However, the mass flow to the southwest part is expected due to the lower elevation. This is verified through the calibration process in which low permeability ($5x10^{-17}$ to $5x10^{-16}$ m^2) is assigned to the blocks in that area and yet still allows fluid to escape.

5.1 Power Output

A production scenario can be estimated to predict the power output from the geothermal system by using the result obtained from the conditioned samples. By integrating the prediction from all sample models, a range of uncertainty value can be calculated based on its probability using P10, P50, and P90 estimates. An algorithm is used to generate these results (Dekkers et al., 2022a; Dekkers et al., 2022b). The objective of the algorithm is to maximise the realistic energy extraction from each sample model. It starts by identifying the potential production and reinjection blocks. The production algorithm iteratively selects target production based on the estimated flow rate using pressure enthalpy curves and the productivity index. These flow rates and pressure enthalpy are updated in each iterative step based on the final state of the reservoir of the last step. This process will continue until the total steam flow rate increases by less than 5% compared to the last step.

Additionally, more production and reinjection wells will be added until the total steam flow rate increases less than 2 kg/s compared to the last step. This is done because it is still viable to drill another production well if the total steam production increases by 2 kg/s (Dekkers et al., 2022a).

The assessment simulates 25 years of production using an assumed separator pressure at 6.5 bar and a conversion rate of 2.5 from steam kg/s to MWe. The result shows that the Kotamobagu geothermal potential is capable of producing at least 70MWe (P90) with a production steam flow rate of approximately 30 kg/s. This scenario is likely to be achieved if the reinjection mass flow rate is kept over 100 kg/s for this period. The probable and possible power potential of the reservoir are 160 MWe (P50) and 270 MWe (P10), respectively. It is worth noting that the extreme samples produced very different amounts of power compared with the P50 result. This highlights that the method captures a wide range of possibilities and provides a robust estimate of the uncertainty.

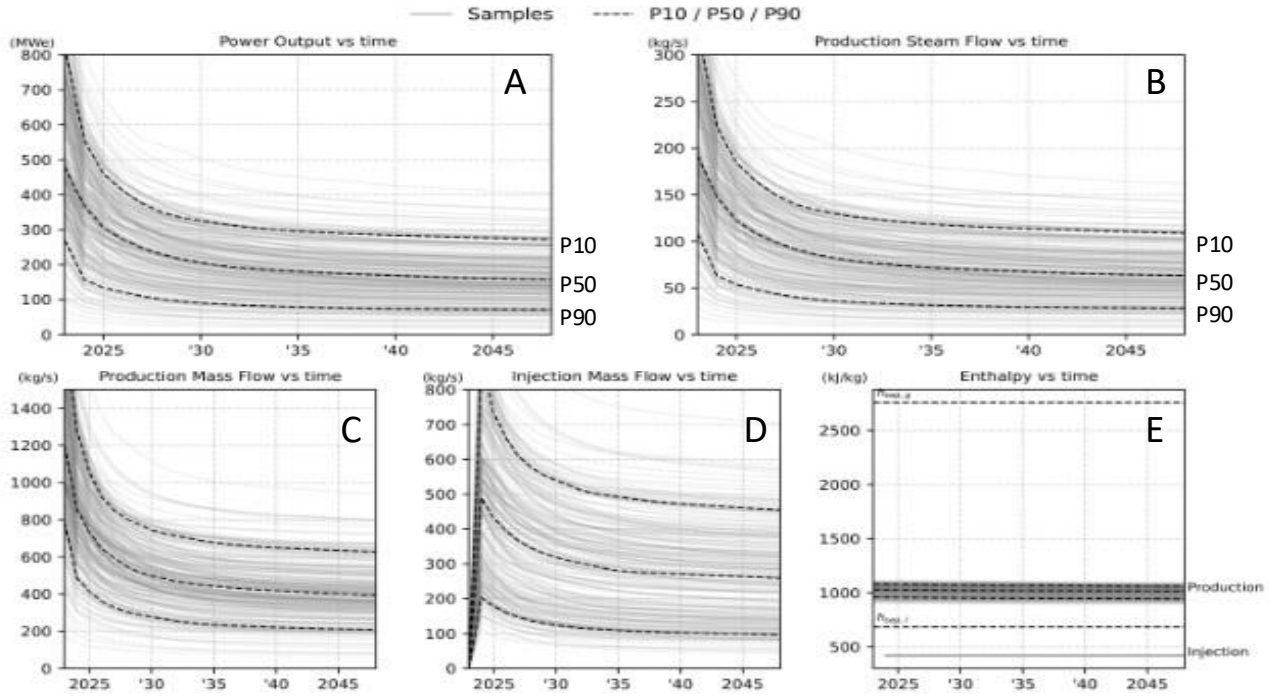

Figure 13: The total resource potential of Kotamobagu Geothermal Field. The graphs show the estimated range for power output (A), steam flow rate (B), production mass flow (C), injection mass flow (D), and enthalpy (D) for 25 years of production. The black dash line shows the P10/P50/P90 obtained from the sample models, while the grey lines show all the sample results.

6. CONCLUSION

This study estimated the resource potential of the Kotamobagu geothermal field in North Sulawesi, Indonesia to be 70MWe (P90) to 270MWe (P10). The result was achieved by incorporating a new, comprehensive 3D natural state model produced by using limited open-source data. The resource is supported by our understanding of the feasible heat source and permeability distribution using uncertainty quantification from an ensemble of acceptable sample models. The approach is expected to give a more accurate estimation of the resource based on the available data.

Based on the challenges experienced on this study, it would be advantageous to have access to the full set of exploration data such as detailed geoscience survey and exploration well data. It would increase confidence in the interpretation of the alteration zone and provide a better understanding on the lithology to reduce uncertainty in allocating the rock type for the numerical model. Downhole measurements also would help to further reduce the uncertainty in the subsurface temperature when calibrating the model.

Applying the methodology used in this study is very valuable as it provides an accurate resource assessment based on the

ISSN 2703-4275

available data and can be easily updated using new data input from field measurements or existing wells. The seamless operation between constructing the geological model using LEAPFROG Geothermal and its numerical model using AUTOUGH2 and Waiwera supports simple modification of the existing model to be compatible with updated data. Furthermore, applying a more accurate assessment provides stakeholders with increased confidence in the economic potential as the result are based on more realistic parameters.

ACKNOWLEDGEMENTS

The authors would like to acknowledge the assistance of Seequent for their provisions of research license for Leapfrog Geothermal, and the use of New Zealand eScience Infrastructure (NeSI) high performance computing facilities as part of this research.

REFERENCES

A. Andan. (1982). *Scientific Studies of the Kotamobagu Geothermal Prospect*.

Apandi, T., & Bachri, S. (1997). *Peta Geologi Lembar Kotamobagu, Sulawesi*.

Boseley, C., Cumming, W., Urzúa-Monsalve, L., Powell, T., & Grant, M. (2010). A Resource Conceptual Model for the Ngatamariki Geothermal Field Based on Recent Exploration Well Drilling and 3D MT Resistivity Imaging. In *Proceedings World Geothermal Congress.*

Cumming, W. (2009, May). Geothermal resource conceptual models using surface exploration data. *34th Workshop on Geothermal Reservoir Engineering*.

De Beer, A., Gravatt, M. J., Renaud, T., Nicholson, R., Maclaren, O. J., Dekkers, K., O'Sullivan, J. P., Power, A., Popineau, J., & O'Sullivan, M. J. (2023). Geologically Consistent Prior Parameter Distributions for Uncertainty Quantification of Geothermal Reservoirs. *48th Workshop on Geothermal Reservoir Engineering*.

Dekkers, K., Gravatt, M., Maclaren, O. J., Nicholson, R., Nugraha, R., O'Sullivan, M., Popineau, J., Riffault, J., & O'Sullivan, J. (2022a). Resource Assessment: Estimating the Potential of a Geothermal Reservoir. *47th Workshop on Geothermal Reservoir Engineering*.

Dekkers, K., Gravatt, M., Renaud, T., Maclaren, O., Renaud, T., De Beer, A., Power, A., Maclaren, O. J., Nicholson, R., O'Sullivan, M., Riffault, J., & O'Sullivan, J. (2022b). Resource Assessment: Estimating the Potential of an African Rift Geothermal Reservoir. *9th African Rift Geothermal Confrence*. https://www.researchgate.net/publication/369453330

Direktorat Panas Bumi. (2017). *Potensi Panas Bumi Indonesia Jilid 2 (Geothermal Potential of Indonesia 2nd Edition)* (2nd ed.).

GoogleEarth. (2023). *Google Earth - Kotamobagu Area*. https://earth.google.com/web/@0.73133549,124.42044754,18524.81856378a,0d,35y,-0.0949h,1.8415t,-0.0000r?utm_source=earth7&utm_campaign=vine&hl=en

Henley, R. W., & Ellis, A. J. (1983). Geothermal Systems Ancient and Modern: A Geochemical Review. In *Earth-Science Reviews* (Vol. 19).

Hochstein, M. P., & Sudarman, S. (2008). History of geothermal exploration in Indonesia from 1970 to 2000. *Geothermics*, *37*(3), 220–266. https://doi.org/10.1016/j.geothermics.2008.01.001

Katili, J. A. (1978). Past and Present Geotectonic Position of Sulawesi, Indonesia. *Tectonophysics*, *45*, 289–322.

Kavalieris, I., Leeuweni, T. M. Van, Wilson~, M., & Kalosi, P. T. (1992). Geological setting and styles of mineralization, north arm of Sulawesi, Indonesia. In *Journal of Southeast Asian Earth Sciences* (Vol. 7, Issue 3).

Patuti, I. M., Rifa'i, A., & Suryolelono, K. B. (2017). *Mechanism and characteristic of the landslide in Bone Bolango regency, Gorontalo Province, Indonesia*.

Popineau, J., O'Sullivan, J., O'Sullivan, M., Archer, R., & Williams, B. (2018). An integrated Leapfrog/TOUGH2 workflow for a geothermal production modelling. *7th African Rift Geothermal Confrence*.

Pruess, K., Oldenburg, C., & Moridis, G. (1999). *TOUGH2 USER'S GUIDE, VERSION 2*.

Riogilang, H., Itoi, R., & Taguchi, S. (2013). Conceptual Model of Hydrothermal System at Kotamobagu Geothermal Field, North Sulawesi, Indonesia. *Procedia Earth and Planetary Science*, *6*, 83–90. https://doi.org/10.1016/j.proeps.2013.01.012

Riogilang, H., Itoi, R., Taguchi, S., Yamashiro, R., Yamashita, S., & Masloman, H. 3. (2011a). Geochemical Study of Hot Spring Water Discharging on the Northern Slope Mt. Muayat in The Kotamobagu Geothermal Fields, North Sulawesi, Indonesia. *Proceedings of the 9th Asian Geothermal Symposium*.

Riogilang, H., Itoi, R., Taguchi, S., Yamashiro, R., Yamashita, S., & Masloman, H. 3. (2011b). Geochemical Study on Hot Spring Water in Kotamobagu geothermal Field, North Sulawesi, Indonesia. *PROCEEDINGS, Thirty-Sixth Workshop on Geothermal Reservoir Engineering*.

Riogilang, H., Itoi, R., Tanaka, T., & Jalilinasrabady, S. (2012, November). *Natural State Model of the Kotamobagu Geothermal System, North Sulawesi, Indonesia.*

van Leeuwen, T. M., & Muhardjo. (2005). Stratigraphy and tectonic setting of the Cretaceous and Paleogene volcanic-sedimentary successions in northwest Sulawesi, Indonesia: Implications for the Cenozoic evolution of Western and Northern Sulawesi. *Journal of Asian Earth Sciences*, *25*(3), 481–511. https://doi.org/10.1016/j.jseaes.2004.05.004

West Japan Engineering Consultants. (2007). *Master Plan Study for Geothermal Power Development in the Republic of Indonesia-Final Report*.